ACTA IMEKO
ISSN: 2221-870X
March 2020, Volume 9, Number 1, 1 - 8

3D shape measurement techniques for human body reconstruction

Iva Xhimitiku[1], Giulia Pascoletti[2], Elisabetta M. Zanetti[3], Gianluca Rossi[3]

[1] *Centro di Ateneo di Studi e Attività Spaziali G. Colombo (CISAS), University of Padua, Via Venezia 15- 35131 Padua, Italy*
[2] *Department of Mechanical and Aerospace Engineering (DIMEAS), Politecnico di Torino, Corso Duca degli Abruzzi 24 - 10129 Turin, Italy*
[3] *Department of Engineering, University of Perugia, Via G. Duranti 93 - 06125, Perugia, Italy*

ABSTRACT

In this work the performances of three different techniques for 3D scanning have been investigated. In particular two commercial tools (smartphone camera and iPad Pro LiDAR) and a structured light scanner (Go!SCAN 50) have been used for the analysis. First of all, two different subjects have been scanned with the three different techniques and the obtained 3D model were analysed in order to evaluate the respective reconstruction accuracy.

A case study involving a child was then considered, with the main aim of providing useful information on performances of scanning techniques for clinical applications, where boundary conditions are often challenging (i.e., non-collaborative patient). Finally, a full procedure for the 3D reconstruction of a human shape is proposed, in order to setup a helpful workflow for clinical applications.

Section: RESEARCH PAPER

Keywords: : 3D scanning techniques; Non-contact measurement; Low cost technology; Customised orthopaedic brace; Non-collaborative patient; Multimodal approach; 3D printing

Citation: Thomas Bruns, Dirk Röske, Paul P. L. Regtien, Francisco Alegria , Template for an Acta IMEKO paper, Acta IMEKO, vol. A, no. B, article C, Month Year, identifier: IMEKO-ACTA-A (Year)-B-C

Section Editor: name, affiliation

Received month day, year; **In final form** month day, year; **Published** Month Year

Funding: [Optional, if applicable] This work was supported by Measurement Science Consultancy, The Netherlands.

Corresponding author: Paul P. L. Regtien, e-mail: paul@regtien.net

1. INTRODUCTION

Biomedical applications often required device customization: as well known, no patient is identical to another one, and this is even truer referring to pathologic conditions. In the past, customization has often been sacrificed in favour of manufacturability, however, with the advent of 3D printing [1], this shortcoming is being overcome [2][3], and more and more emphasis is being given to the necessity of providing fast and accurate systems to obtain the geometry of the whole body [4] [5] [6] or of specific body segments [7]. Traditional techniques are based on plaster moulds and are affected by some major limitations such as: the invasiveness, the need to keep the patient still for the curing time [8], a limited accuracy (over 15 mm, according to [9], [10]), and the impossibility of acquiring undercut geometries. More recently, and as a viable alternative, various non-contact instruments have been developed in order to perform digital scanning [11] [12] [13] and the respective performances have been extensively reported in literature [14] [15]. However, the application introduced in this work was somehow peculiar due to the young age of the patient [16] which led to add some requirements to the scanning methodology that are a time limit to perform the whole acquisition, and the possibility to compensate motions since the patient was not collaborative due to his young age [17] [18]. The final aim was obtaining the 3D geometry of his trunk in order to gather input data for brace design[19]. Prior attempts had been made with traditional moulding techniques and they did not succeed due to frequent patient movements [20] [21] [22]. A specific methodology has been here developed, tested and discussed, which is based on a multimodal approach [23] where the benefits of different scanning technique are merged in order to optimize the final result.

In the following 'Background' section three common scanning techniques are briefly described, reporting their specifications, and highlighting the respective advantages and disadvantages in relation to their application to human body

scanning. These technologies are photogrammetry, light detection and ranging (LiDAR) and structured light scan.

The performances of these shape measurement techniques have been assessed reconstructing the torso of two adults (one male and one female); the main objective of this first analysis was to evaluate the performances of two low-cost tools [16] [24] [25] (smartphone camera and iPad Pro LiDAR), in relation to the accurate reconstruction obtainable with the structured light scanner, used as reference measurement system [26]. Once the performances of these tools have been defined under 'ideal' scanning conditions (collaborative subject able to maintain a position throughout the scan process), the same techniques have been used to obtain a set of 3D scans of a 4-year-old boy's torso, at an orthopaedic laboratory (Officina Ortopedica Semidoro srl, Perugia, ITALY).

For both these analyses, the process of 3D reconstruction and structure extraction is described in detail in the 'Results' section. The accuracy and correlation among the geometries reconstructed with different visual devices, are evaluated and discussed, and the bias given by a non-collaborative patient is illustrated, leading to introduce a new methodology based on a multimodal approach, whose benefit are outlined and quantified.

In the 'Discussion' section it is demonstrated how this methodology can be applied in orthopaedics [1] [8] [11], and on least collaborative patients, making it possible to obtain body scans where the alternative based on plaster of Paris moulds would fail or would result in lower accuracy and longer execution times.

2. BACKGROUND

Techniques here used to perform body scans include different technologies; herein photogrammetry, structured light and LiDAR will be considered (Figure 1).

a) Photogrammetry (PH): it is an imaging method used to capture pictures of objects from different perspectives with calibrated cameras. The feature points obtained by overlapped images are used to calculate shooting position through specific algorithms which allow individuating automatically chromatic analogies between two images [21] [27] [28].
b) LiDAR: recent developments of commercial devices such as smartphones and tablets have led to very fast scanning with LiDAR. This technique is based on Time of Flight (ToF) [29] measurements, that is the time taken by an object, a particle or a wave to travel a certain distance. More specifically, LiDAR emits a pulse or modulated light signal and measures the time difference in the returning wavefront [25] [30]; this allows estimating distance from signal propagation speed.
c) Structured Light scanner (SL): this technology is based on the projection of a known light pattern (grid) on the object and, according to the deformation of this projected grid on the curved surface of the object, reconstructs its geometry. Moreover, triangulation is used for the location of each point on the object, thanks to two cameras placed at known angles.

These measurement techniques have some specific advantages over contact measuring techniques, such as fast acquisition, high accuracy, and minimal invasiveness.

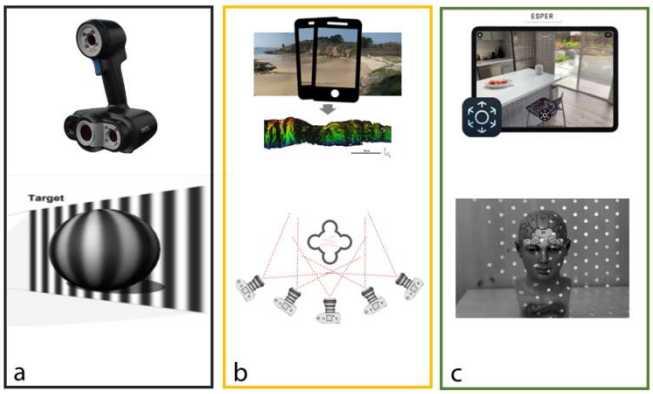

Figure 1. Instruments and operation scheme: a) Structured Light; b) Photogrammetry; c) LiDAR.

Depending on the application, some specifications may become more relevant than others. With reference to clinical applications, in some cases high resolution and accuracy must be prioritized, while in other cases a good representation of the colour and structure is mandatory.

3. INSTRUMENTS

3.1. Photogrammetry

For this application a commercial smartphone Redmi Note 10 with an average cost of 190 € was used. It is equipped with a duo camera system dedicated for commercial use. Its technology includes a digital stabilizer, 30 fps video speed and Video rec. 4K (2160p). This tool has been paired to Zephyr software (3D Flow, v. Aerial 3.1) in order to obtain a 3D reconstruction. This software uses Structure from Motion (SfM) algorithms for photogrammetric processing of digital images to create 3D spatial data.

3.2. Structured light scanner

The Go!SCAN 50 (15k€) is a hand-held scanner based on structured light with high speed. In total, this scanner uses three cameras positioned at various angles and depths. In the centre of the device, an RGB camera is installed surrounded by LED flash light to capture textures without the need for special light setup. The scanner works at a rate of 550000 measurements per second, covering a scanning area of 380×380 mm with a resolution of 0.5 mm and a point accuracy up to 0.1 mm. A lamp guidance system helps to set the scanning distance between 0.3 and 3.0 m. The surface is captured while moving the hand-held scanner over the object. Moreover, it is possible to reduce the noise arising from movement, by setting the appropriate parameters on the acquisition software (VX Element by Creaform, v. 0.9) [31]. The Go!SCAN 50 is the only certified instrument among those used for this work; for this reason, the respective reconstructed 3D geometries have been considered as the most accurate for replicating the actual torso shape and used as reference to evaluate the reconstruction accuracy of the other techniques [32] [33].

3.3. LiDAR

The iPad Pro LiDAR scanner is a pulsed laser able to capture surroundings up to 5 m through a photon-level reading since it works at time of flight, the time required for data acquisition is strictly related to the speed of light and distance. Apple itself does not specify the accuracy of the respective technologies or hardware [25]. This tool allows scanning objects

and exporting scans as 3D textured CAD models. The scanning resolution used for our applications was 0.2 mm.

The scanning time for a particular subject varies from operator to operator since using each scanner is an acquired skill. In general, scanning could take about 15 min depending on the desired accuracy level of the resulting scan [14]. As a rule of thumb, the fastest technique is the LiDAR scanning and the slowest one is the SL system. Subject comfort is comparable among the reviewed scanners.

4. METHODOLOGY

In the first part of this work the accuracy of reconstruction of the scanning techniques here considered was investigated through the trunk reconstruction of a male and a female human subject. Scanning results coming from this analysis have been used as reference for techniques comparison, since the subjects can be considered in a stable configuration, with the exception of the intrinsic deformability of the trunk (micro movements due to breathing). In the following step, the same analysis has been repeated on a 4-year-old trunk, adding one more bias given by subject's macro-movements.

PH is characterised by a timing video acquisition of about 50 s for each subject. Using Zephyr software, the geometry of the torso was reconstructed taking a total of 7 h with high software settings: up to 15000 keypoints per image and Pairwise image matching setting on at least 10 images. Keypoints are specific points in a picture that Zephyr can understand and recognize in different pictures. Matching stage depth (Pairwise image matching) controls how many pairwise image matching to perform. Usually, the more is the better, however, this comes at a computational cost.

The mesh given by this scan technique can result in shape's topological errors due to shadow areas and object's movement. The shape complexity and the macro movements led to sudden changes of curvature, making the reconstruction difficult and resulting so in missing parts and loss of details.

The mesh obtained from the scan performed with Go!SCAN 50 required higher manual processing times, given the computational heaviness due to the high resolution. The scan parameters were set directly in the VX Elements software according to the manufacturer, with a resolution of 2 mm. Targets, semi-rigid positioning, and natural features were used for placement parameters.

The acquisition and processing data both required an average time of 15 min under ideal conditions (collaborative subject).

Scanning with the iPad is the fastest technique. Accurate colour information (texture) can be obtained from the two rear cameras whose images are managed by proprietary algorithms. Output meshes are of low quality, due to the limited number of triangles used for the surface discretization.

For both adults and child scanning analyses, the procedure consists of four main steps:

1) Scanning:

Trunk acquisition required the scanners to rotate around the subject; adhesive circular reference targets with a diameter of 10 mm have been used in order to facilitate the alignment and matching between scans on the post-processing phase (Figure 2 b); these targets have been positioned over the trunk considering that, as well known, at least three tie-points must be present in two neighbouring scans in order to allow the respective alignment.

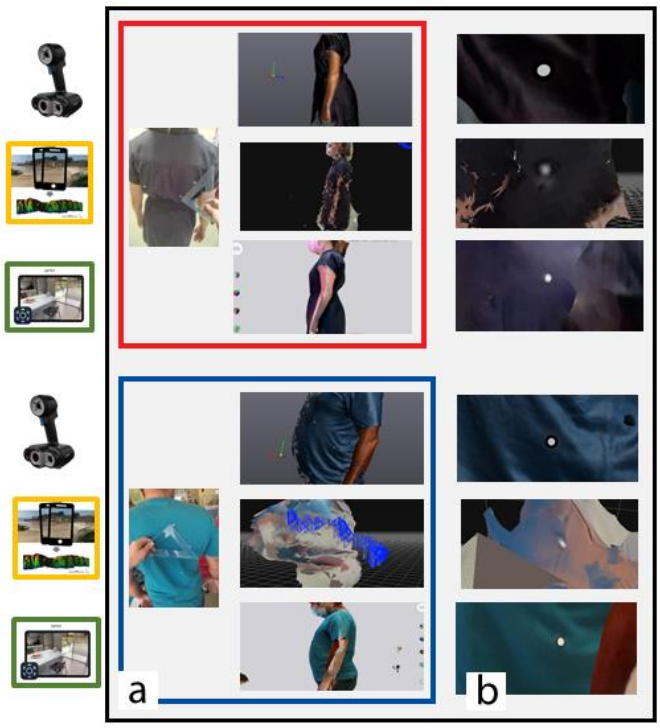

Figure 2. Data obtained by acquisition with the three instruments; a) Body reconstruction of a female and a male (red and blue); b) Marker details.

2) Geometry reconstruction (post-processing):

Post-processing was performed using Geomagic Studio Software (3D System, v. 12) [34]. Sometimes, data acquisition results in more than one point cloud, so these point clouds have to be registered and then merged in order to obtain one single cloud. A cleaning phase follows, where spurious points are eliminated; these points are generated by environment noise and by subject motion or by the camera resolution being close to the size of geometric details. A triangulated mesh is then generated, and it is smoothed to obtain a more regular geometry. The smoothing phase must be performed carefully in order to avoid losing relevant information. Finally, the mesh is edited to avoid double vertices, discontinuities of face's normal, holes, internal faces, so obtaining a manifold geometry. At the end of editing, the mesh is optimised to reduce the number of triangles.

3) Comparison among measurement techniques:

First of all, scanners' performances were evaluated in terms of times required to obtain the final geometry.

The geometries were then compared through a fully automated operation, performed by dedicated software: Geomagic Studio. It should be reminded that mesh coming from different scanning are not iso-topological [25] and this can make this operation more critical in addition to the 288389, 431000, 158000 triangles being processed for male, female and child torso respectively.

More in detail, for the adults' scans case, the reference geometry obtained from Go!SCAN 50 was compared to output geometries from PH and from LiDAR, analysing the distribution of distances both before and after mesh filtering. A software-coded mapping analysis between pairwise scans was performed: results of this analysis are represented by the standard deviation of the statistical distribution of the shortest distance between two scans, along with the mean value of this distance. This analysis is a signed type analysis; for this reason,

Table 1. Comparison of distances' distributions between LiDAR and SL scans, for the adult case.

Pairwise comparison between techniques	Reference Scan	Max (mm)	Mean +/- (mm)	Dev. Std. (mm)	Distant point (%)
SL_LiDAR (Female subject)	SL	20	7.61/5.42	8.63	17
SL_PH (Female subject)	SL	20	12.52/11.06	13.14	57
SL_LiDAR (Male subject)	SL	20	6.00/7.00	9.00	38
SL_PH (Male subject)	SL	20	15.00/14.00	16.00	94

in the following positive and negative values of the mean distance will be provided, representing deviations towards the outer or inner scanned volume, respectively (Figure 3).
For the child torso (Figure 4), this deviation analysis was performed twice. In the first instance, LiDAR scans were compared, analysing the deviation distribution at different threshold levels (10, 20, 80, 120 and 180 mm), where the threshold parameter represents the distance value (in mm) beyond which the mesh points are considered as outliers. This analysis was performed because three LiDAR scans were obtained: a full body scan (longer acquisition time) and two partial body scans (shorter acquisition time). Over the

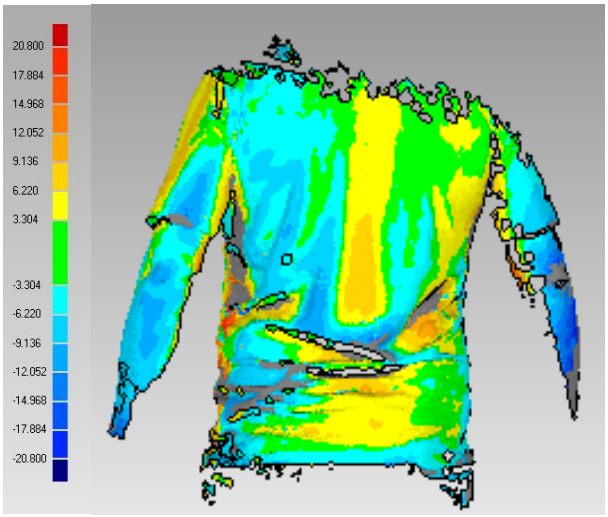

Figure 3. Example of distances' distributions between the outputs obtained with SL and LiDAR instruments: male torso.

acquisition time of the two partial scans, the subject's torso could be reasonably considered still, while the full body scan, due to the longer acquisition time, was more biased by macro movements. The multimodal approach used for the child torso consists in the reconstruction of the 3D geometry using the two partial SL scans after their alignment with the LiDAR scan, which was used as a reference for the global alignment, since it was the only technique which allowed obtaining a full body scan. The deviation analysis among LiDAR models has allowed quantifying full scan's macro movements and the respective reconstruction uncertainty for the final torso 3D model, if this scan was used as reference for the Go!SCAN 50 model positioning.
4) Measurement:
Prior to subjects' trunk scanning, some main measurements were taken with a seamstress meter in order to have a reference when checking the scanned geometry scale.

5. RESULTS

5.1. Adult subjects scan

Scans from SL scanner are the most accurate and are certified; therefore, as aforementioned, they were used as a reference.

For PH, it was possible to reconstruct only a portion of the surface for the female subject, while meshes related to the male test has resulted without detail: 94% of points were too far from SL points to be used for the calculation of geometric deviation (Figure 3). With reference to the female subject, 57% of points resulted to be far from the SL model. This is due to male subject movement, colour and reflection of clothes. The best matching points were located at the torso back.

LiDAR scans were more complete: only 17% of points had to be discarded for the female subject and 38% for the male one (Table 1).

In terms of triangles number, which is closely related to the geometry accuracy, SL scan has given a total of 350614 triangles, PH has resulted in 14430 triangles, and LiDAR has provided 37792 triangles for the male subject and 46811 triangles for the female subject. Two reference points have been tracked through apposite markers (Figure 2 b).

The respective distance was equal to 100 mm with reference to the male subject, and 90 mm for the female subject. In the male subject this same distance was evaluated equal to 98.6 mm with SL (1.49% uncertainty); 109 mm with LiDAR (9% uncertainty). With reference to the female subject, the respective distance was evaluated equal to 89.9 mm with SL (1.11% uncertainty), and 104 mm with LiDAR (15.5% uncertainty).

Figure 4. a) Young child torso and detail of scan's output given by b) PH, c) LiDAR and d) SL techniques.

Table 2. Comparison of distances' distributions between LiDAR scans for the child case.

Pairwise comparison between three LiDAR scans	Reference Scan	Max (mm)	Mean +/- (mm)	Dev. Std. (mm)	Distant point (%)
LiDAR 1 (Young boy)	LiDAR 2	20	7.60/9.54	10.00	57
LiDAR 2 (Young boy)	**LiDAR 3**	**20**	**8.27/7.52**	**9.16**	**44**
LiDAR 3 (Young boy)	**LiDAR 1**	**20**	**6.05/5.97**	**7.90**	**13**

5.2. Young boy's Scans

The following information has been obtained:

a) 1 PH scan, with partial covering of the subject's trunk, obtained in 18 s with 110244 triangles (referred as 'PH' in the following);

b) 3 LiDAR scans: one full-body scan (biased by the movement of the subject) with 8420 triangles and two partial scans of the left (4310 triangles) and right side (4303 triangles), minimally affected by child's movements. These scans required 4 s and 10 s for the left and the right side, and 20 s for the full trunk. In the following, these scans are referred to as LiDAR '1', '2' and '3' (left, right and full-body respectively), according to the respective position in the scanning sequence (Figure 5);

c) 2 partial SL scans from Go!SCAN 50: these are much more accurate (47294 triangles) and required about 5 min for the back side and 4 min for front side.

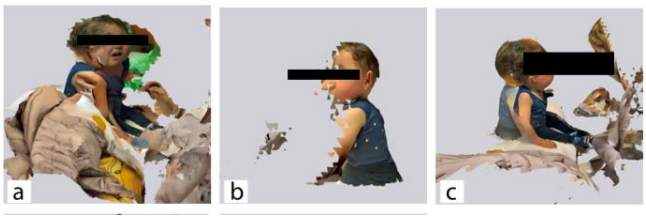

Figure 5. LiDAR acquisition: a) right side scan detail of three LiDAR scan acquisitions referred to as 'LiDAR 1'; b) left side scan without movement, referred to as 'LiDAR 2'; c) total body scan movement, referred to as 'LiDAR 3'.

PH failed to reconstruct the trunk because the legs were the only still part of the child's body (Figure 4 b).

5.2.1. Analysis of LiDAR's results

In Figure 6 a detail of LiDAR scans alignment is shown.

Figure 6. Example of LiDAR scans alignment: a) point selection for alignment; b) alignment; c) top view of alignment.

The three scans were compared through three pairwise combinations, varying the threshold distance: the distribution of distances between two scans has been obtained on a limited set of points, whose distance laid below this given threshold value. This threshold has been varied in order to assess its influence on final results (Figure 7).

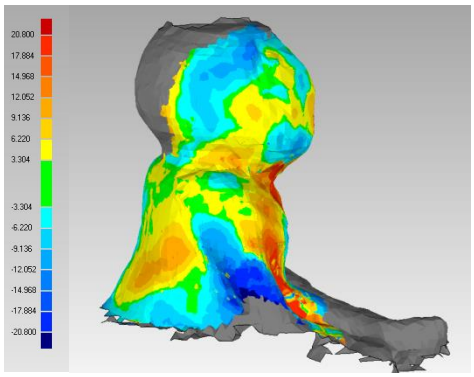

Figure 7. Example of Pairwise comparisons between LiDAR 1 and LiDAR 6 scans with a threshold value of 20 mm. Green colour indicates areas with below-threshold distances, red areas are above the reference surface and blue ones are below the reference surface, grey areas are out of range (outlier).

According to Figure 8a, 10 mm or 20 mm threshold values have to be chosen in order to keep the standard deviation below 60 mm. However, 10 mm threshold would produce a too high percentage of outliers, as shown in Figure 8 b.

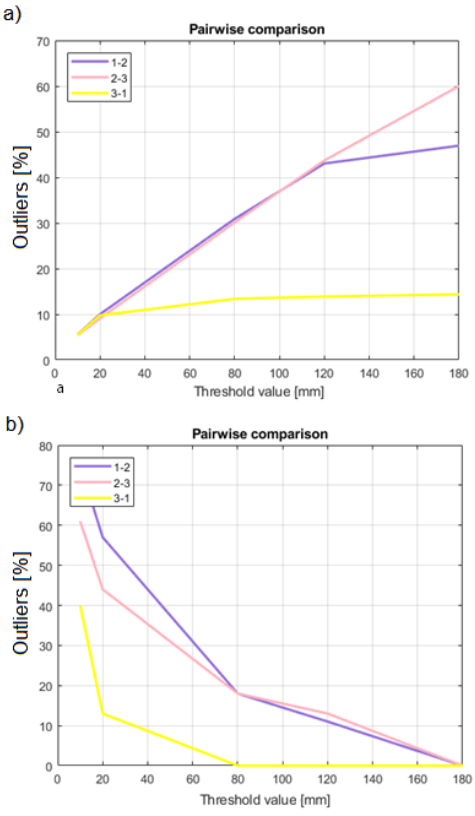

Figure 8. Trend of a) standard deviation and b) percentage of outliers versus threshold values for different pairwise comparisons.

Table 3. Comparisons between Structured Light and LiDAR scans for the child.

Techniques	Reference Scan	Max (mm)	Mean +/- (mm)	Dev. Std. (mm)	Distant point (%)
SL_LiDAR 1	SL	20	6.73/5.83	6.68	55
SL_LiDAR 2	SL	20	5.71/5.49	6.65	75
SL_LiDAR 3	SL	20	6.32/6.93	6.93	62

Therefore, a threshold value equal to 20 mm has been chosen: it represents the trade-off between the standard deviation and the percentage of retained points.

Having chosen the 20 mm threshold as reference, the mean values for the standard deviation of distances among LiDAR scans have been analysed. These values are reported in Table 2: they show that the minimum value of the deviation is associated to LiDAR 2 (which is the fastest scan) versus LiDAR 3 comparison and LiDAR 3 (which is the only full body scan available) versus LiDAR 1 comparison (bolded values in Table 2). For this reason, LiDAR 3 has been chosen as a reference for the following alignment procedure in multimodal scans.

5.2.2. LiDAR versus Structured Light

Scans from SL have been considered as a reference since the respective scanner has been certified and this technique is known to be the most accurate [33].

An optimized geometric alignment was performed by Geomagic Studio software, which is based on Iterative Closest Point algorithms. Figure 9 show the displacement between scans after alignment. The sections are evaluated by a level curves measurement tool that returns the circumferences of trunk.

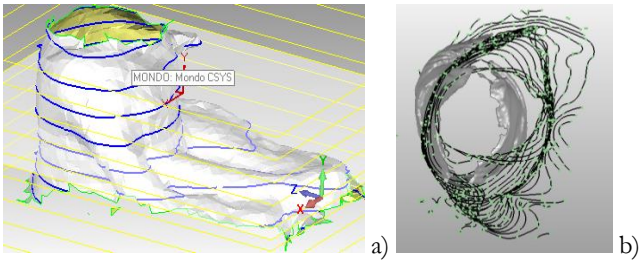

Figure 9. a) Level curves (blue curves) for distance evaluation between LiDAR and SL scans: b) Example of LiDAR 3 to SL scan alignment.

Three combinations have been studied: three scans form LiDAR were compared to both SL scans (Figure 10).

The maximum standard deviation has resulted to be equal to 6.93 mm with mean values equal to +6.32 mm and -6.36 mm (where positive and negative values represent deviations towards the outer or inner scanned volume, respectively) obtained from SL-LiDAR 3 combination, corresponding to the overlap between the full LiDAR and the SL scans (reference). On the other hand, the minimum standard deviation is represented by overlapping the fastest LiDAR scan (LiDAR 2) and both partial SL scans (references).

The value of standard deviation in this case is 6.65 mm with mean values equal to +5.71 mm and -5.49 mm (Table 3).

As noted, the full body LiDAR scan (LiDAR 3) has the closest values to both SL scans and it is the best suited to replicate the actual back shape and to be used as reference for SL scans alignment.

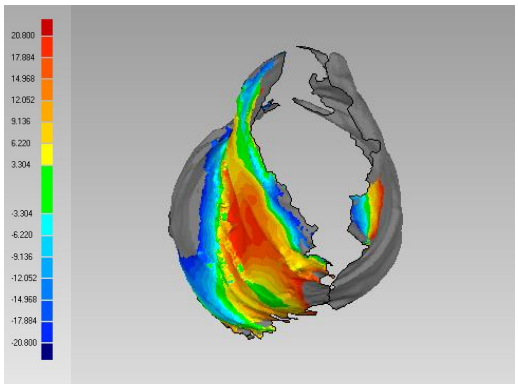

Figure 10. Example of distances distribution between SL and LiDAR 3 scan.

5.2.3. Multimodal procedure

The full body scan obtained from LiDAR was used as reference for both SL scans (chest and back) positioning, while PH provided an incomplete result which could not be merged to obtain a full trunk scan. Looking at LiDAR results, the lines of movement can be outlined in texture scans (Figure 11).

Figure 11. LiDAR movement texture detail. Upper Row: side view. Lower Row: back view. a) Column: LiDAR 1; b) Column: LiDAR 2 scan; c) Column: LiDAR 3.

The two SL scans were overlapped on the 3D LiDAR full scan and in the next step a topological optimization of the trunk was performed with 3-Matic (Materialise, v. 12) [35], a software used for clinical application (Figure 12).

Finally, a comparison between the actual trunk measurements (circumferences at chest and waist levels) and the corresponding measurements taken on the reconstructed geometry was performed, resulting in a difference of 5.9 mm (1.25%) at the waist level, and an uncertainty of 8.2 mm (1.64%) at the chest level (Figure 13).

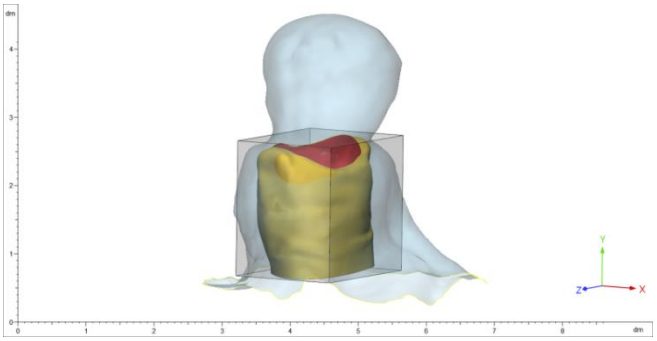

Figure 12. Reconstruction of torso in 3-Matic Materialise, using the full LiDAR scan as a reference.

The plaster mould accuracy, acceptable for medical applications is above 15 mm [9], [10]. The uncertainty of the reconstruction for this multimodal non-contact measurement methodology is within this limits in fact the maximum uncertainty is 8.2 mm.

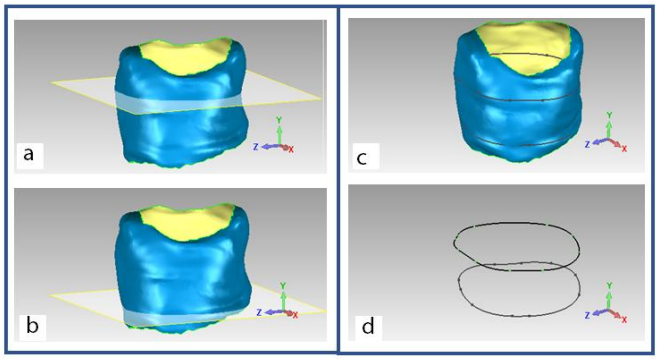

Figure 13. Reconstruction of torso and measurement of a) circumferences at chest and b) waist levels c) Intersection between an horizontal plane and model. d) Level curves to be measured.

6. DISCUSSION

All instruments, photogrammetry, structured light scanner and LiDAR have been proved to be able to capture trunk geometry in a still patient; when results coming from all three instruments were compared to those coming from traditional techniques based on plaster moulding, they proved to be more accurate with the advantage of producing a digital editable model. Structured light scanner produced the most accurate results.

When a non-collaborative patient is considered, new specifications must be taken into account such as the time required for scanning the whole geometry and the robustness of reconstruction algorithms. As a result, LiDAR technique was proved to be the only technique able to provide a full scan, thanks to the lowest acquisition time. However, the respective accuracy was quite low and LiDAR could not be used alone; however, it could be used as reference for structured light scans registration, so removing the major source of noise in SL, that is non-collaborative patient's movement.

From this, it can be pointed out that a multimodal methodology was needed in order to overcome the limited accuracy of LiDAR, recovering information from partial scans obtained from SL. The whole methodology has been set up and tested with encouraging results: the final outcome has an acceptable accuracy (8.2 mm), where the only alternative would be taking a limited number of measurements on the non-collaborative patient body. Compared to plaster moulding, the accuracy is greatly improved (8.2 mm against 15 mm), and the bias given by dermal tissue compressibility [36], [37] is totally absent.

Once the scans were cleaned, simplified and merged, the Standard Triangulation Language (STL) model was exported and 3D printed, to evaluate the viability of this workflow to produce a customised brace. Finally, the brace was manufactured with traditional method on the 3D printed volume, without any contact with the subject (Figure 14), after having been virtually tested through mock up techniques [38].

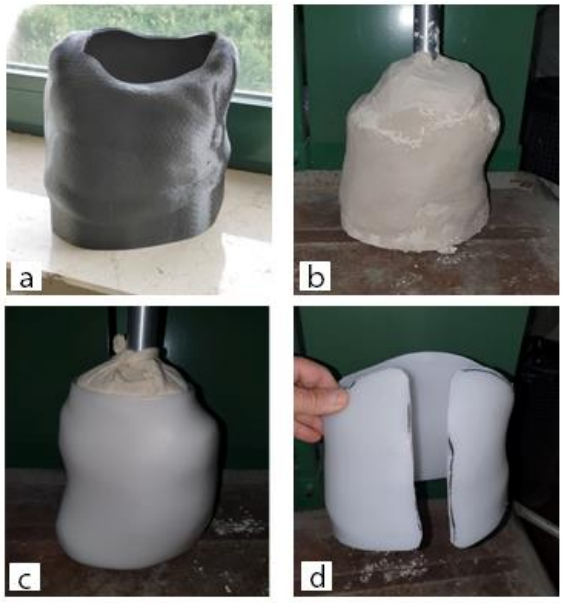

Figure 14. a) 3D printed trunk, b) Plaster mould built on printed model, c) Plaster realization d) Final model.

7. CONCLUSIONS

In this work a multimodal scanning approach was proposed. The uncertainty given by movement was analysed and compensated. A full procedure for the reconstruction of the 3D external shape was developed by integration of different 3D measurement techniques. The shape of the human torso of a child was finally measured, 3D printed and used for the creation of a patient-specific brace.

Future developments will focus on combining fast and low-cost techniques and algorithms with low-cost measurement systems for orthopaedic applications, in order to improve the measurement technique without the need for high-performance tools.

ACKNOWLEDGEMENT

This research did not receive any specific grant from funding agencies in the public, commercial, or not-for-profit sectors.

REFERENCES

[1] D. F. Redaelli *et al.*, "3D printing orthopedic scoliosis braces: a test comparing FDM with thermoforming," *Int. J. Adv. Manuf. Technol.*, vol. 111, no. 5–6, pp. 1707–1720, 2020, doi: 10.1007/s00170-020-06181-1.

[2] M. Calì, G. Pascoletti, A. Aldieri, M. Terzini, G. Catapano, and E. M. Zanetti, "Feature-Based Modelling of Laryngoscope Blades for Customized Applications," in *Advances on Mechanics, Design Engineering and Manufacturing III*, 2021, pp. 206–211.

[3] M. Calì, G. Pascoletti, M. Gaeta, G. Milazzo, and R. Ambu, "A new generation of bio-composite thermoplastic filaments for a

more sustainable design of parts manufactured by FDM," *Appl. Sci.*, vol. 10, no. 17, 2020, doi: 10.3390/app10175852.

[4] S. Grazioso, M. Selvaggio, and G. Di Gironimo, "Design and development of a novel body scanning system for healthcare applications," *Int. J. Interact. Des. Manuf.*, vol. 12, no. 2, pp. 611–620, 2018, doi: 10.1007/s12008-017-0425-9.

[5] F. Remondino, "3-D reconstruction of static human body shape from image sequence," *Comput. Vis. Image Underst.*, vol. 93, no. 1, pp. 65–85, 2004.

[6] J. Tong, J. Zhou, L. Liu, Z. Pan, and H. Yan, "Scanning 3D full human bodies using kinects," *IEEE Trans. Vis. Comput. Graph.*, vol. 18, no. 4, pp. 643–650, 2012, doi: 10.1109/TVCG.2012.56.

[7] N. Tokkari *et al.*, "Comparison and use of 3D scanners to improve the quantification of medical images (surface structures and volumes) during follow up of clinical (surgical) procedures," *Adv. Biomed. Clin. Diagnostic Surg. Guid. Syst. XV*, vol. 10054, p. 100540Z, 2017, doi: 10.1117/12.2253241.

[8] P. Andrés-Cano, J. A. Calvo-Haro, F. Fillat-Gomà, I. Andrés-Cano, and R. Perez-Mañanes, "Role of the orthopaedic surgeon in 3D printing: current applications and legal issues for a personalized medicine," *Rev. Esp. Cir. Ortop. Traumatol.*, vol. 65, no. 2, pp. 138–151, 2021, doi: 10.1016/j.recot.2020.06.014.

[9] M. Farhan, J. Z. Wang, P. Bray, J. Burns, and T. L. Cheng, "Comparison of 3D scanning versus traditional methods of capturing foot and ankle morphology for the fabrication of orthoses: a systematic review," *J. Foot Ankle Res.*, vol. 14, no. 1, pp. 1–11, 2021, doi: 10.1186/s13047-020-00442-8.

[10] W. Clifton, M. Pichelmann, A. Vlasak, A. Damon, K. ReFaey, and E. Nottmeier, "Investigation and Feasibility of Combined 3D Printed Thermoplastic Filament and Polymeric Foam to Simulate the Cortiocancellous Interface of Human Vertebrae," *Sci. Rep.*, vol. 10, no. 1, pp. 1–9, 2020, doi: 10.1038/s41598-020-59993-2.

[11] J. C. Rodríguez-Quiñonez *et al.*, "Optical monitoring of scoliosis by 3D medical laser scanner," *Opt. Lasers Eng.*, vol. 54, pp. 175–186, 2014, doi: 10.1016/j.optlaseng.2013.07.026.

[12] D. G. Chaudhary, R. D. Gore, and B. W. Gawali, "Inspection of 3D Modeling Techniques for Digitization," *Int. J. Comput. Sci. Inf. Secur. (IJCSIS),* vol. 16, no. 2, pp. 8–20, 2018.

[13] P. Dondi, L. Lombardi, M. Malagodi, and M. Licchelli, "3D modelling and measurements of historical violins," *Acta IMEKO*, vol. 6, no. 3, pp. 29–34, 2017, doi: 10.21014/acta_imeko.v6i3.455.

[14] C. Boehnen and P. Flynn, "Accuracy of 3D scanning technologies in a face scanning scenario," *Proc. Int. Conf. 3-D Digit. Imaging Model. 3DIM*, pp. 310–317, 2005, doi: 10.1109/3DIM.2005.13.

[15] P. Treleaven and J. Wells, "3D body scanning and healthcare applications," *Computer (Long. Beach. Calif).*, vol. 40, no. 7, pp. 28–34, 2007, doi: 10.1109/MC.2007.225.

[16] C. Pérez *et al.*, "Data-driven three-dimensional reconstruction of human bodies using a mobile phone app," *Int. J. Digit. Hum.*, vol. 1, no. 4, p. 361, 2016, doi: 10.1504/ijdh.2016.10005376.

[17] M. Pesce, L. M. Galantucci, G. Percoco, and F. Lavecchia, "A low-cost multi camera 3D scanning system for quality measurement of non-static subjects," *Procedia CIRP*, vol. 28, pp. 88–93, 2015, doi: 10.1016/j.procir.2015.04.015.

[18] R. F. de Oliveira *et al.*, "Enhanced Reader.pdf," *Nature*, vol. 388. pp. 539–547, 2018.

[19] I. Molnár and L. Morovič, "Design and manufacture of orthopedic corset using 3D digitization and additive manufacturing," *IOP Conf. Ser. Mater. Sci. Eng.*, vol. 448, no. 1, 2018, doi: 10.1088/1757-899X/448/1/012058.

[20] F. Remondino and A. Roditakis, "3D reconstruction of human skeleton from single images or monocular video sequences," *Lect. Notes Comput. Sci. (including Subser. Lect. Notes Artif. Intell. Lect. Notes Bioinformatics)*, vol. 2781, pp. 100–107, 2003, doi: 10.1007/978-3-540-45243-0_14.

[21] J. A. Beraldin, "Basic theory on surface measurement uncertainty of 3D imaging systems," *Three-Dimensional Imaging Metrol.*, vol. 7239, p. 723902, 2009, doi: 10.1117/12.804700.

[22] V. Rudat, P. Schraube, D. Oetzel, D. Zierhut, M. Flentje, and M. Wannenmacher, "Combined error of patient positioning variability and prostate motion uncertainty in 3D conformal radiotherapy of localized prostate cancer," *Int. J. Radiat. Oncol. Biol. Phys.*, vol. 35, no. 5, pp. 1027–1034, 1996, doi: 10.1016/0360-3016(96)00204-0.

[23] J. A. Torres-Martínez, M. Seddaiu, P. Rodríguez-Gonzálvez, D. Hernández-López, and D. González-Aguilera, "A multi-data source and multi-sensor approach for the 3D reconstruction and web visualization of a complex archaelogical site: The case study of 'Tolmo De Minateda,'" *Remote Sens.*, vol. 8, no. 7, 2016, doi: 10.3390/rs8070550.

[24] L. Barazzetti, L. Binda, M. Scaioni, and P. Taranto, "Photogrammetric survey of complex geometries with low-cost software: Application to the 'G1' temple in Myson, Vietnam," *J. Cult. Herit.*, vol. 12, no. 3, pp. 253–262, 2011, doi: 10.1016/j.culher.2010.12.004.

[25] M. Vogt, A. Rips, and C. Emmelmann, "Comparison of iPad Pro®'s LiDAR and TrueDepth Capabilities with an Industrial 3D Scanning Solution," *Technologies*, vol. 9, no. 2, p. 25, 2021, doi: 10.3390/technologies9020025.

[26] I. Xhimitiku, G. Rossi, L. Baldoni, R. Marsili, and M. Coricelli, "Critical analysis of instruments and measurement techniques of the shape of trees: Terresrial Laser scanner and Structured Light scanner," in *2019 IEEE International Workshop on Metrology for Agriculture and Forestry, MetroAgriFor 2019 - Proceedings*, Oct. 2019, pp. 339–343, doi: 10.1109/MetroAgriFor.2019.8909215.

[27] M. Lo Brutto and G. Dardanelli, "Vision metrology and Structure from Motion for archaeological heritage 3D reconstruction: A Case Study of various Roman mosaics," *Acta IMEKO*, vol. 6, no. 3, pp. 35–44, 2017, doi: 10.21014/acta_imeko.v6i3.458.

[28] C. Buzi *et al.*, "Measuring the shape: Performance evaluation of a photogrammetry improvement applied to the Neanderthal skull Saccopastore 1," *Acta IMEKO*, vol. 7, no. 3, pp. 79–85, 2018, doi: 10.21014/acta_imeko.v7i3.597.

[29] S. Logozzo, A. Kilpelä, A. Mäkynen, E. M. Zanetti, and G. Franceschini, "Recent advances in dental optics - Part II: Experimental tests for a new intraoral scanner," *Opt. Lasers Eng.*, vol. 54, pp. 187–196, Mar. 2014, doi: 10.1016/j.optlaseng.2013.07.024.

[30] D. Marchisotti, P. Marzaroli, R. Sala, M. Sculati, H. Giberti, and M. Tarabini, "Automatic measurement of hand dimensions using consumer 3D cameras," *Acta IMEKO*, vol. 9, no. 2, pp. 75–82, 2020, doi: 10.21014/acta_imeko.v9i2.706.

[31] M. Di and M. Di, "Piattaforma software 3d completamente integrata," no. Mi, 2020.

[32] L. Ma, T. Xu, and J. Lin, "Validation of a three-dimensional facial scanning system based on structured light techniques," *Comput. Methods Programs Biomed.*, vol. 94, no. 3, pp. 290–298, 2009, doi: 10.1016/j.cmpb.2009.01.010.

[33] A. Cuartero, "Study of uncertainty and repeatability in structured-light 3D scanners," no. 2.

[34] G. Wrap, "Presentazione di Geomagic Wrap 2021," 2021.

[35] R. Guide and M. N. V All, "Version 14.0 – Reference guide," no. April, 2019.

[36] M. Terzini, C. Bignardi, C. Castagnoli, I. Cambieri, E. M. Zanetti, and A. L. Audenino, "Ex vivo dermis mechanical behavior in relation to decellularization treatment length," *Open Biomed. Eng. J.*, vol. 10, pp. 34–42, 2016, doi: 10.2174/1874120701610010034.

[37] M. Terzini, C. Bignardi, C. Castagnoli, I. Cambieri, E. M. Zanetti, and A. L. Audenino, "Dermis mechanical behaviour after different cell removal treatments," *Med. Eng. Phys.*, vol. 38, no. 9, pp. 862–869, 2016, doi: 10.1016/j.medengphy.2016.02.012.

[38] E. M. Zanetti and C. Bignardi, "Mock-up in hip arthroplasty pre-operative planning," *Acta Bioeng. Biomech.*, vol. 15, no. 3, pp. 123–128, 2013, doi: 10.5277/abb130315.